Analytical Methods

PAPER

View Article Online
View Journal

Cite this: DOI: 10.1039/c6ay00199h

Deciphering the quenching mechanism of 2D MnO_2 nanosheets towards Au nanocluster fluorescence to design effective glutathione biosensors†

Shichao Lin,‡[a] Hanjun Cheng,‡[ab] Qiran Ouyang[a] and Hui Wei*[a]

Two-dimensional (2D) nanomaterials (such as 2D MnO_2 nanosheets) have received increasing attention due to their unique photophysical properties, rich redox chemistry, excellent colloidal stability, good biocompatibility, *etc.* Recently, numerous sensing platforms have been reported by exploring the 2D MnO_2 nanosheet mediated fluorescence quenching towards fluorophores and/or redox reactions between MnO_2 and reductive targets. Though various fluorophores have been used in 2D MnO_2 nanosheet based turn-on sensing systems, ultrasmall metal nanoclusters have not been exploited yet. Furthermore, the quenching mechanisms of MnO_2 nanosheets towards various fluorophores have remained elusive. To address these issues, we studied the quenching of Au nanocluster fluorescence by 2D MnO_2 nanosheets. First, we demonstrated that 2D MnO_2 nanosheets were effective quenchers towards the fluorescence of metal nanoclusters (*e.g.*, AuNC@BSA, the bovine serum albumin stabilized Au nanocluster). We further revealed that both dynamic and static quenching effects played critical roles in the quenching process while fluorescence resonance energy transfer (FRET) and inner filter effect (IFE) only played very minor roles in the quenching process. Finally, we developed a turn-on sensing strategy for detection of glutathione (GSH), an important antioxidant with good sensitivity and selectivity. This work provides useful insights in understanding the mechanisms of nanomaterial-induced fluorescence quenching. It also paves a way to design turn-on fluorescent sensors for important reductive targets.

Received 20th January 2016
Accepted 12th April 2016

DOI: 10.1039/c6ay00199h

www.rsc.org/methods

Introduction

Two-dimensional (2D) nanomaterials have received considerable attention due to their intriguing structures and properties.[1–15] Until now, various kinds of 2D nanomaterials have been developed, such as graphene, germanane, silicene, phosphorene, boron nitride, transition metal chalcogenide, layered double hydroxide, transition metal oxide, and their derivatives.[16–18] Among them, ultrathin transition metal oxide nanosheets are of great interest owing to their rich redox chemistry, good biocompatibility, ease of functionalization, and low cost.[19]

Particularly, MnO_2 nanosheets have recently been fabricated for broad applications such as in catalysis, biosensing, bioimaging, and cancer therapy.[20–32] MnO_2 nanosheets have a unique sandwich structure, with one Mn atomic layer located between two O atomic layers.[20] Thus, an edge-sharing octahedral conformation of MnO_6 is adopted through coordination between Mn atom and six O atoms.[20] As a consequence of the d–d transition of Mn ions in the MnO_6 octahedra, MnO_2 nanosheets exhibit a broad absorption band (~200–800 nm) with a large molar extinction coefficient (*i.e.*, $\varepsilon_{max} = 9.6 \times 10^3$ M^{-1} cm^{-1} at ~380 nm).[20] On the other hand, the presence of Mn vacancies endows MnO_2 nanosheets with a negatively charged surface, which in turn provides MnO_2 nanosheets with good colloidal stability due to the electrostatic repulsion. Such interesting properties allow researchers to construct platforms for fluorescence sensing. For example, when a dye-labelled single-stranded DNA (ssDNA) was used as a probe, its fluorescence was quenched by MnO_2 nanosheets.[33] In the presence of target ssDNA, the formation of a DNA duplex could recover the quenched fluorescence, resulting in sensitive and selective detection of the target ssDNA.[33] Such a sensing strategy could also be applied for RNA detection as well as other targets' detection with corresponding aptamer probes.[27,32,33] Furthermore, by combining the interesting redox chemistry of MnO_2 nanosheets with their fluorescence quenching capability, various biologically important targets with reducing ability (such as ascorbic acid, glutathione (GSH), H_2O_2, *etc.*) have been detected.[34,35] For instance, the fluorescence of 7-hydroxycoumarin was suppressed by MnO_2 nanosheets. In the presence of a reductive analyte (*i.e.*, ascorbic acid), MnO_2 nanosheets

[a]Department of Biomedical Engineering, College of Engineering and Applied Sciences, Collaborative Innovation Center of Chemistry for Life Sciences, Nanjing National Laboratory of Microstructures, Nanjing University, Nanjing 210093, China. E-mail: weihui@nju.edu.cn

[b]State Key Laboratory of Analytical Chemistry for Life Science, Nanjing University, Nanjing 210093, China

† Electronic supplementary information (ESI) available. See DOI: 10.1039/c6ay00199h

‡ These authors contributed equally.

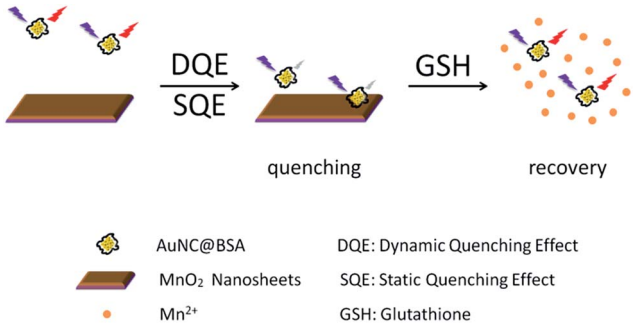

Fig. 1 2D MnO_2 nanosheet mediated Au nanocluster fluorescence quenching for effective glutathione detection.

could be reduced to Mn^{2+}, thus liberating 7-hydroxycoumarin and restoring its fluorescence. Based on this strategy, ascorbic acid in living rats has been successfully determined.[34] GSH, an important endogenous antioxidant, has also been detected based on a similar sensing strategy by several groups.[22]

Compared with organic dye-based fluorophores, ultrasmall fluorescent metal nanoclusters are advantageous in several aspects, such as ultrasmall size, remarkable photophysical and chemical stability, high fluorescence, tunable emissions, *etc.*[36–51] Therefore, they are promising alternatives to organic dyes for constructing turn-on fluorescent sensors with functional nanomaterials. For example, when DNA-stabilized Ag nanoclusters were combined with graphene oxide, multiplexed sensing platforms for pathogenic DNA were developed recently.[52]

Despite the great promise, no reports have been devoted to the construction of turn-on fluorescent sensing platforms with MnO_2 nanosheets and ultrasmall metal nanoclusters. On the other hand, the quenching mechanisms of MnO_2 nanosheets towards various fluorescent reporters for turn-on fluorescent sensors have also remained largely unexplored.[22,25,27,34] The elucidation of such mechanisms would enable us to rationally design effective fluorescent sensors for targets of interest. In this work, we aim at understanding the quenching mechanism of 2D MnO_2 nanosheets towards protein stabilized Au nanocluster fluorescence, which in turn allows us to design effective turn-on fluorescent sensors for GSH detection (Fig. 1).

Experimental section

Chemicals and materials

Bovine serum albumin (BSA) (Biosharp Company), $HAuCl_4$ (Nanjing Chemical Reagent Co., Ltd), NaOH (Nanjing Chemical Reagent Co., Ltd), $MnCl_2 \cdot 4H_2O$ (Xilong Chemical Co., Ltd), glutathione (GSH) (Aladdin Industrial Corporation), H_2O_2 (Nanjing Aojia Chemical Co., Ltd), tetramethylammonium (TMA) (Nanjing Aojia Chemical Co., Ltd), and all other chemicals were of analytical grade and used as received. All aqueous solutions were prepared with deionized water (18.2 MΩ cm, Millipore).

Instrumentation

Absorption spectra were recorded at room temperature on a TU 1900 spectrometer (Beijing Purkinje General Instrument Co. Ltd., China). Photoluminescence spectra were measured on a Hitachi F-4600 spectrometer (Hitachi Co. Ltd., Japan) with an excitation wavelength at 365 nm. Transmission electron microscopy (TEM) images were acquired on a JEM-2100 transmission electron microscope at the acceleration voltage of 200 kV.

Preparation of BSA stabilized gold nanoclusters

BSA stabilized gold nanoclusters (AuNC@BSA) were prepared as follows.[53] Typically, 5 mL of 10 mM $HAuCl_4$ aqueous solution was added into 5 mL of 50 mg mL^{-1} BSA aqueous solution under vigorous stirring at 37 °C. Two minutes later, 0.5 mL of 1 M NaOH aqueous solution was added and the resulting reaction solution was stirred at 37 °C overnight. The as-prepared AuNC@BSA was stored at 4 °C for further usage.

Preparation of ultrathin 2D MnO_2 nanosheets

Ultrathin 2D MnO_2 nanosheets were prepared as follows.[20] First, 12 mL of 1 M TMA and 2 mL of 30% H_2O_2 were mixed into 6 mL of water. Then the mixed solution of 0.6 M TMA and 3% H_2O_2 was rapidly added into 10 mL of 0.3 M $MnCl_2$ aqueous solution under vigorous stirring at room temperature. After overnight vigorous stirring in open air, the dark brown products were collected by centrifugation (2000 rpm, 20 minutes) and purified by washing with water and methanol. The products were then dried in a vacuum oven at 60 °C and stored for further experiments. To get well-dispersed MnO_2 nanosheets in water, the stocking MnO_2 nanosheets were ultrasonicated for at least 10 h before using them.

The concentration of MnO_2 nanosheets was calculated with the molar extinction coefficient of 9.6×10^3 M^{-1} cm^{-1} at 380 nm.[20]

Fluorescence quenching of AuNC@BSA by MnO_2 nanosheets

To investigate the potential mechanisms of the ultrathin MnO_2 nanosheet-induced fluorescence quenching of AuNC@BSA, the same volume of ultrathin MnO_2 nanosheets with different concentrations was added into AuNC@BSA (20 μM). Then the fluorescence intensity of the mixed solution was recorded with an excitation wavelength of 365 nm.

Glutathione detection

GSH detection was carried out as follows. First, the same volume of ultrathin MnO_2 nanosheets (800 μM) was added into AuNC@BSA (20 μM) to completely quench the fluorescence of the AuNC@BSA. Then, GSH with various concentrations was added to 1 mL of the above solution to recover the fluorescence of AuNC@BSA. The recovered fluorescence was measured to qualify the GSH concentration with an excitation wavelength of 365 nm.

Results and discussion

Quenching fluorescence of AuNC@BSA with MnO_2 nanosheets

AuNC@BSA was prepared using a previously reported method.[53] The as-prepared AuNC@BSA emitted reddish fluorescence under UV lamp irradiation (data not shown). The AuNC@BSA

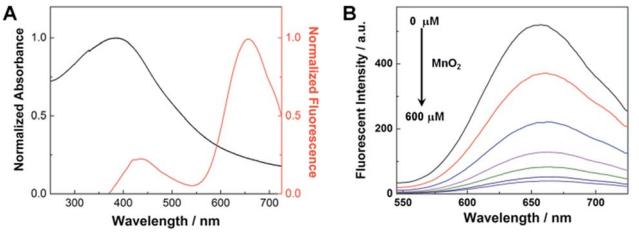

Fig. 2 Quenching fluorescence of AuNC@BSA with MnO_2 nanosheets. (A) Normalized UV-visible absorption spectrum of MnO_2 nanosheets (black curve) and fluorescence emission spectrum of AuNC@BSA (red curve). (B) Fluorescence quenching of AuNC@BSA by varying amounts of MnO_2 nanosheets. The concentrations of MnO_2 nanosheets were 0, 100, 200, 300, 400, 500, and 600 μM (from top to bottom). λ_{ex} = 365 nm.

exhibited dual emissions at 430 nm and 653 nm when excited at 365 nm (Fig. 2A). This is consistent with previous results.[49,53] The 2D MnO_2 nanosheets were obtained *via* a one-step approach.[20] The successful formation of 2D MnO_2 nanosheets was confirmed by TEM imaging, which clearly revealed the formation of large ultrathin 2D sheet structures with irregular folds and wrinkles (Fig. S1†). The UV-visible absorption spectra showed a broad absorption band (ranging from 250 nm to 725 nm with a peak centered at around 380 nm), which originated from the d–d transition of Mn ions in the MnO_6 octahedra (Fig. 2A).[20]

Since the absorption spectra of MnO_2 nanosheets well overlapped with the emission spectra of AuNC@BSA from 550 nm to 725 nm, we reasoned that the presence of MnO_2 nanosheets would effectively quench the fluorescence of AuNC@BSA. As shown in Fig. 2B, the titration of MnO_2 nanosheets into AuNC@BSA indeed gradually quenched the fluorescence. Such an interesting phenomenon can be further explored for constructing a turn-on fluorescence sensor for GSH detection (Fig. 1 and discussion *vide infra*).

Mechanism of MnO_2 nanosheets towards AuNC@BSA fluorescence quenching

Usually, there are several possible mechanisms contributing to the quenching of a fluorescence reporter by nanomaterials, such as fluorescence resonance energy transfer (FRET), inner filter effect (IFE), dynamic quenching effect (DQE) and static quenching effect (SQE).[54] To understand the exact mechanism responsible for the MnO_2 nanosheet mediated fluorescence quenching of AuNC@BSA, the following studies were carried out.

First, the potential contribution of FRET was investigated since it has been suggested to be responsible for the fluorescence quenching of organic dyes by 2D nanomaterials (*e.g.*, graphene oxide and MnO_2 nanosheets).[22,35,55] The fluorescence quenching efficiency contributed by FRET was calculated under the assumption that the donor (*i.e.* AuNC@BSA) and the acceptor (*i.e.*, MnO_2 nanosheets) were randomly distributed in 3D solutions (see detailed calculation in the ESI†).[54] Both the experimentally observed quenching efficiency and the calculated quenching efficiency contributed *via* FRET for MnO_2 nanosheets at different concentrations are shown in Fig. 3. Even for the highest concentration of MnO_2 nanosheets tested (*i.e.*, 600 μM), the fluorescence could only be quenched by 3.6% *via* FRET. These results clearly indicated that FRET only played a minor role in the fluorescence quenching process.

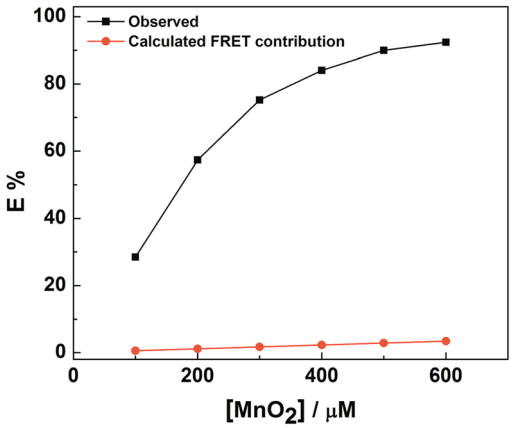

Fig. 3 The observed quenching efficiency (black curve) and the calculated quenching efficiency contributed *via* FRET (red curve) of MnO_2 nanosheets towards AuNC@BSA at different concentrations of MnO_2 nanosheets.

Second, the potential contribution of IFE was considered since the broad absorption spectra of MnO_2 nanosheets overlapped with both the excitation and emission ranges of AuNC@BSA (Fig. 2A). Considering the cuvette geometry we used for the measurement, the quenching efficiency from IFE was carefully analyzed (see detailed analysis in the ESI†). The observed quenching efficiency and the corrected quenching efficiency by excluding the contribution of IFE for different concentrations of MnO_2 nanosheets are plotted in Fig. 4. For all the concentrations of MnO_2 nanosheets measured, there were no significant differences between the observed and the corrected fluorescence quenching efficiencies. These results strongly suggested that IFE was not the main mechanism for the fluorescence quenching process either.

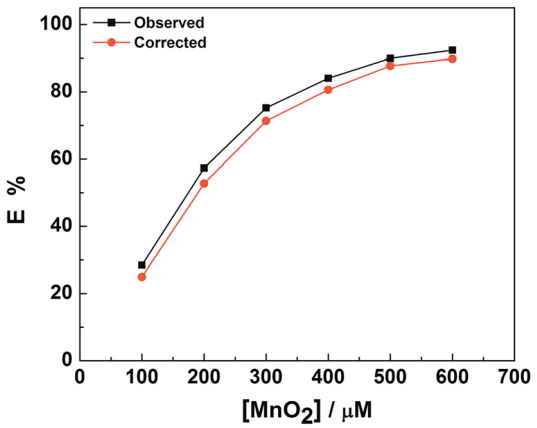

Fig. 4 The observed quenching efficiency (black curve) and the corrected quenching efficiency by excluding the contribution of IFE (red curve) of MnO_2 nanosheets towards AuNC@BSA at different concentrations of MnO_2 nanosheets.

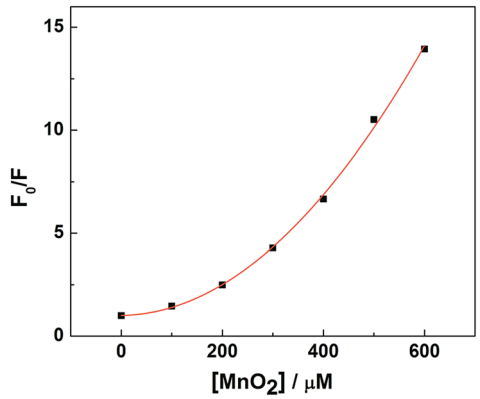

Fig. 5 Stern–Volmer plot of F_0/F *versus* MnO_2 nanosheet concentration after excluding FRET and IFE contributions. F_0, the steady state fluorescence of AuNC@BSA in the absence of MnO_2 nanosheets; F, the steady state fluorescence of AuNC@BSA in the presence of MnO_2 nanosheets.

Then, the contribution of DQE and SQE was studied. As illustrated in Fig. S3,† the contact between the fluorophore and the quencher is required for both dynamic and static quenching.[54] For a dynamic quenching process, the quencher must first diffuse to the fluorophore during the lifetime of the excited state. The fluorophore then returns to the ground state after colliding with the quencher, without emitting a photon.[54] For a static quenching process, on the other hand, a nonfluorescent fluorophore/quencher complex is formed upon collision with each other.[54] Previous studies have established that both DQE and SQE are governed by the Stern–Volmer equation (*i.e.*, eqn (S10) in the ESI†).[54] The F_0/F after removing the FRET and IFE contributions was plotted against the concentration of MnO_2 nanosheets, which exhibited an interesting upward curvature (note, the curve is concaved towards the positive *y*-axis) (Fig. 5). Such a characteristic curve fits well to the modified Stern–Volmer equation (*i.e.*, eqn (S14) in the ESI†), which assumes that both the dynamic and static quenching processes are involved with the same fluorophore (here MnO_2 nanosheets). Note that the modified Stern–Volmer equation is second order in the concentration of the quencher, which was also confirmed by our calculation.

The above results demonstrated that both DQE and SQE mechanisms dominated the fluorescence quenching process of AuNC@BSA by MnO_2 nanosheets while the FRET and IFE mechanisms played almost negligible roles in the fluorescence quenching process.

Sensitive and selective detection of GSH

After elucidating the mechanism responsible for the fluorescence quenching of AuNC@BSA by MnO_2 nanosheets, a turn-on fluorescent sensor for GSH was constructed by exploring the redox reaction between MnO_2 and GSH (Fig. 1). GSH detection is of great importance due to its antioxidant capacity and critical roles in various cellular processes.[56–58] The abnormal levels of GSH are associated with numerous diseases such as neurodegenerative diseases, AIDS, heart diseases and cancer.[22,59–62] Therefore considerable efforts have been devoted to GSH detection by developing facile methods.[22,61,62]

It has been shown that the MnO_2 nanosheet quenched fluorescence could be restored when the MnO_2 nanosheets were reduced to Mn^{2+} with suitable reducing agents.[22,34] In the case of GSH detection, the MnO_2 nanosheets would be reduced to Mn^{2+} by GSH following eqn (1) below. Thus, the quenched fluorescence of AuNC@BSA would be recovered (Fig. 1).

$$MnO_2 + GSH + 2H^+ \rightarrow Mn^{2+} + GSSG + 2H_2O. \quad (1)$$

As depicted in Fig. 6A, the titration of GSH into the mixture of AuNC@BSA and MnO_2 nanosheets gradually recovered the fluorescence. 1.5 mM GSH was needed to saturate the fluorescence recovery by a factor of about 29. The $(F - F_0)/F_0$ showed a good dynamic range for the concentration of GSH from 0.1 mM to 2.0 mM (Fig. 6B), which could cover the intracellular concentrations of GSH.[63] As shown in Fig. 6C, a linear range from 0 mM to 0.5 mM as well as a detection limit of 20 μM towards GSH were obtained. Furthermore, the sensing performance of the current method could be further tuned by using different concentrations of MnO_2 nanosheets (Fig. S4†).

The selectivity of the turn-on sensing system towards GSH detection was also evaluated. As shown in Fig. 6D, the potential interfering chemicals (such as $CaCl_2$, $MnCl_2$, KCl, NaCl, glycine, $MgSO_4$, PBS, fructose, proline, glucose, and Tris–HCl) with 100 times the concentration of GSH did not significantly affect the

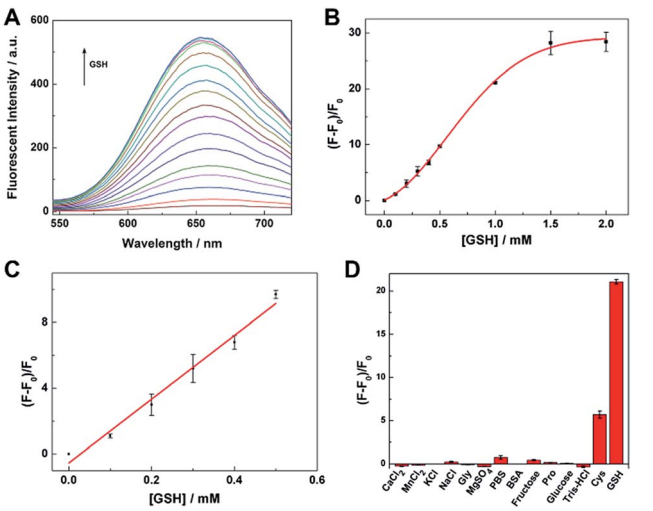

Fig. 6 Sensitive and selective detection of GSH using 800 μM MnO_2 nanosheets. (A) Fluorescence titration profile of AuNC@BSA/MnO_2 nanosheets with an increasing amount of GSH (from bottom to top, 0.0 to 2.0 mM with an interval of 0.1 mM). (B) Plot of $(F - F_0)/F_0$ *versus* GSH concentration. (C) Linear response of $(F - F_0)/F_0$ to GSH concentration. (D) Selective detection of 1 mM GSH in the presence of potential interfering components. The concentration of $CaCl_2$, $MnCl_2$, KCl, NaCl, glycine, $MgSO_4$, PBS, fructose, proline, glucose, and Tris–HCl was 100 mM, the concentration of BSA was 0.1 mg mL^{-1}, the concentration of cysteine was 1 mM, and the concentration of GSH was 1 mM. F_0 and F are the fluorescent intensities of the sensing system in the absence and presence of GSH (or other potential interfering chemicals), respectively. Error bars indicate standard deviations of three independent measurements.

detection. 0.1 mg mL^{-1} for BSA did not interfere with the detection either. Cysteine, the free thiol containing amino acid, could also turn on the fluorescence. For example, 1 mM Cys restored the fluorescence by 5.7 folds. However, considering the much lower cellular concentration of Cys (around tens to hundreds μM level), the presence of Cys would not affect the GSH detection either.[64,65] These results demonstrated that the proposed turn-on sensing strategy exhibited good sensitivity and selectivity towards GSH detection.

Conclusions

In this study, we have demonstrated that 2D MnO_2 nanosheets were effective quenchers towards the fluorescence of metal nanoclusters (such as AuNC@BSA). Moreover, the mechanisms responsible for the fluorescence quenching were systematically investigated. It was found that both DQE and SQE mechanisms dominated the fluorescence quenching process of AuNC@BSA by MnO_2 nanosheets while the FRET and IFE mechanisms played very minor roles in the fluorescence quenching process. This is different from the previous reports, which suggested that the quenching mainly originated from FRET and/or IFE.[27] Such a difference may be due to the distinct nature of fluorophores used (*i.e.*, organic dyes *versus* metal nanoclusters). Furthermore, a sensitive and selective turn-on fluorescent sensing system for GSH detection was demonstrated based on the redox reactions between MnO_2 and reductive GSH. This study may be helpful in understanding the mechanisms of nanomaterial-mediated fluorescence quenching. It also paves a way to design turn-on fluorescent sensors for important reductive targets.[66]

Acknowledgements

This work was supported by National Natural Science Foundation of China (21405079, 21405081), Natural Science Foundation of Jiangsu Province (BK20130561), 973 Program (2015CB659400), PAPD program, Fundamental Research Funds for Central Universities (no. 20620140617 and 20620140627), Shuangchuang Program of Jiangsu Province, Six Talents Summit Program of Jiangsu Province, Open Funds of the State Key Laboratory of Electroanalytical Chemistry (SKLEAC201501), Open Funds of the State Key Laboratory of Analytical Chemistry for Life Science (SKLACLS1404) and Thousand Talents Program for Young Researchers.

References

1 C. Zhu, J. Zhai and S. Dong, *Nanoscale*, 2014, **6**, 10077–10083.
2 K. S. Novoselov, A. K. Geim, S. V. Morozov, D. Jiang, Y. Zhang, S. V. Dubonos, I. V. Grigorieva and A. A. Firsov, *Science*, 2004, **306**, 666–669.
3 S. J. Guo and S. J. Dong, *Chem. Soc. Rev.*, 2011, **40**, 2644–2672.
4 E. Gibney, *Nature*, 2015, **522**, 274–276.
5 Y. Shi, J. Wang, C. Wang, T.-T. Zhai, W.-J. Bao, J.-J. Xu, X.-H. Xia and H.-Y. Chen, *J. Am. Chem. Soc.*, 2015, **137**, 7365–7370.
6 L. Wu, L. Zeng and X. Jiang, *J. Am. Chem. Soc.*, 2015, **137**, 10052–10055.
7 L. Gao, L.-L. Li, X. Wang, P. Wu, Y. Cao, B. Liang, X. Li, Y. Lin, Y. Lu and X. Guo, *Chem. Sci.*, 2015, **6**, 2469–2473.
8 M. Chhowalla, Z. F. Liu and H. Zhang, *Chem. Soc. Rev.*, 2015, **44**, 2584–2586.
9 G. Guan, S. Zhang, S. Liu, Y. Cai, M. Low, C. P. Teng, I. Y. Phang, Y. Cheng, K. L. Duei, B. M. Srinivasan, Y. Zheng, Y.-W. Zhang and M.-Y. Han, *J. Am. Chem. Soc.*, 2015, **137**, 6152–6155.
10 Y. M. Shi, J. K. Huang, L. M. Jin, Y. T. Hsu, S. F. Yu, L. J. Li and H. Y. Yang, *Sci. Rep.*, 2013, **3**, 1839.
11 A. Berkdemir, H. R. Gutierrez, A. R. Botello-Mendez, N. Perea-Lopez, A. L. Elias, C. I. Chia, B. Wang, V. H. Crespi, F. Lopez-Urias, J. C. Charlier, H. Terrones and M. Terrones, *Sci. Rep.*, 2013, **3**, 1755.
12 H. Wei and E. K. Wang, *Chem. Soc. Rev.*, 2013, **42**, 6060–6093.
13 J. N. Coleman, M. Lotya, A. O'Neill, S. D. Bergin, P. J. King, U. Khan, K. Young, A. Gaucher, S. De, R. J. Smith, I. V. Shvets, S. K. Arora, G. Stanton, H.-Y. Kim, K. Lee, G. T. Kim, G. S. Duesberg, T. Hallam, J. J. Boland, J. J. Wang, J. F. Donegan, J. C. Grunlan, G. Moriarty, A. Shmeliov, R. J. Nicholls, J. M. Perkins, E. M. Grieveson, K. Theuwissen, D. W. McComb, P. D. Nellist and V. Nicolosi, *Science*, 2011, **331**, 568–571.
14 M. Zhou, Y. Zhai and S. Dong, *Anal. Chem.*, 2009, **81**, 5603–5613.
15 H. Zhang, *ACS Nano*, 2015, **9**, 9451–9469.
16 B. Dubertret, T. Heine and M. Terrones, *Acc. Chem. Res.*, 2015, **48**, 1–2.
17 J. Sun, S. W. Yang, Z. Y. Wang, H. Shen, T. Xu, L. T. Sun, H. Li, W. W. Chen, X. Y. Jiang, G. Q. Ding, Z. H. Kang, X. M. Xie and M. H. Jiang, *Part. Part. Syst. Charact.*, 2015, **32**, 434–440.
18 Y. Zhang, Y. M. Guo, Y. L. Xianyu, W. W. Chen, Y. Y. Zhao and X. Y. Jiang, *Adv. Mater.*, 2013, **25**, 3802–3819.
19 L. Z. Wang and T. Sasaki, *Chem. Rev.*, 2014, **114**, 9455–9486.
20 K. Kai, Y. Yoshida, H. Kageyama, G. Saito, T. Ishigaki, Y. Furukawa and J. Kawamata, *J. Am. Chem. Soc.*, 2008, **130**, 15938–15943.
21 Y. Yoshida, K. Kai, H. Kageyama and G. Saito, *J. Mater. Chem.*, 2011, **21**, 5863–5866.
22 R. R. Deng, X. J. Xie, M. Vendrell, Y. T. Chang and X. G. Liu, *J. Am. Chem. Soc.*, 2011, **133**, 20168–20171.
23 X. Liang, C. Hart, Q. Pang, A. Garsuch, T. Weiss and L. F. Nazar, *Nat. Commun.*, 2015, **6**, 5682.
24 H. M. Meng, Z. Jin, Y. F. Lv, C. Yang, X. B. Zhang, W. H. Tan and R. Q. Yu, *Anal. Chem.*, 2014, **86**, 12321–12326.
25 Z. L. Zhao, H. H. Fan, G. F. Zhou, H. R. Bai, H. Liang, R. W. Wang, X. B. Zhang and W. H. Tan, *J. Am. Chem. Soc.*, 2014, **136**, 11220–11223.
26 Y. Chen, D. L. Ye, M. Y. Wu, H. R. Chen, L. L. Zhang, J. L. Shi and L. Z. Wang, *Adv. Mater.*, 2014, **26**, 7019–7026.
27 C. X. Wang, W. Y. Zhai, Y. X. Wang, P. Yu and L. Q. Mao, *Analyst*, 2015, **140**, 4021–4029.
28 Y. H. Wang, K. Jiang, J. L. Zhu, L. Zhang and H. W. Lin, *Chem. Commun.*, 2015, **51**, 12748–12751.

29 H. M. Meng, L. M. Lu, X. H. Zhao, Z. Chen, Z. L. Zhao, C. Yang, X. B. Zhang and W. H. Tan, *Anal. Chem.*, 2015, **87**, 4448–4454.
30 H. H. Fan, Z. L. Zhao, G. B. Yan, X. B. Zhang, C. Yang, H. M. Meng, Z. Chen, H. Liu and W. H. Tan, *Angew. Chem., Int. Ed.*, 2015, **54**, 4801–4805.
31 H. Wang, J. J. Zhang, X. D. Hang, X. D. Zhang, J. F. Xie, B. C. Pan and Y. Xie, *Angew. Chem., Int. Ed.*, 2015, **54**, 1195–1199.
32 Y. X. Yuan, S. F. Wu, F. Shu and Z. H. Liu, *Chem. Commun.*, 2014, **50**, 1095–1097.
33 D. G. He, X. X. He, K. M. Wang, X. Yang, X. X. Yang, X. C. Li and Z. Zou, *Chem. Commun.*, 2014, **50**, 11049–11052.
34 W. Y. Zhai, C. X. Wang, P. Yu, Y. X. Wang and L. Q. Mao, *Anal. Chem.*, 2014, **86**, 12206–12213.
35 J. Yuan, Y. Cen, X. J. Kong, S. Wu, C. L. W. Liu, R. Q. Yu and X. Chu, *ACS Appl. Mater. Interfaces*, 2015, **7**, 10548–10555.
36 J. Zhu, L. Zhang, Y. Teng, B. Lou, X. Jia, X. Gu and E. Wang, *Nanoscale*, 2015, **7**, 13224–13229.
37 J. Li, X. Jia, D. Li, J. Ren, Y. Han, Y. Xia and E. Wang, *Nanoscale*, 2013, **5**, 6131–6138.
38 W. Wei, Y. Lu, W. Chen and S. Chen, *J. Am. Chem. Soc.*, 2011, **133**, 2060–2063.
39 Y. Lu and W. Chen, *Chem. Soc. Rev.*, 2012, **41**, 3594–3623.
40 Y. Lu and W. Chen, *Anal. Chem.*, 2015, **87**, 10659–10667.
41 L. Jin, Y. Fang, L. Shang, Y. Liu, J. Li, L. Wang, P. Hu and S. Dong, *Chem. Commun.*, 2013, **49**, 243–245.
42 L. Zhang, J. Zhu, Z. Zhou, S. Guo, J. Li, S. Dong and E. Wang, *Chem. Sci.*, 2013, **4**, 4004–4010.
43 L. Shang, S. J. Dong and G. U. Nienhaus, *Nano Today*, 2011, **6**, 401–418.
44 H. Wei, Z. D. Wang, L. M. Yang, S. L. Tian, C. J. Hou and Y. Lu, *Analyst*, 2010, **135**, 1406–1410.
45 C. L. Guo and J. Irudayaraj, *Anal. Chem.*, 2011, **83**, 2883–2889.
46 T. Chen, Y. Hu, Y. Cen, X. Chu and Y. Lu, *J. Am. Chem. Soc.*, 2013, **135**, 11595–11602.
47 L. Shang, F. Stockmar, N. Azadfar and G. U. Nienhaus, *Angew. Chem., Int. Ed.*, 2013, **52**, 11154–11157.
48 Y. B. Ding, L. L. Shi and H. Wei, *J. Mater. Chem. B*, 2014, **2**, 8268–8291.
49 Y. H. Hu, W. J. Guo and H. Wei, *Isr. J. Chem.*, 2015, **55**, 682–697.
50 F. Wen, Y. H. Dong, L. Feng, S. Wang, S. C. Zhang and X. R. Zhang, *Anal. Chem.*, 2011, **83**, 1193–1196.
51 H. Kong, Y. X. Lu, H. Wang, F. Wen, S. C. Zhang and X. R. Zhang, *Anal. Chem.*, 2012, **84**, 4258–4261.
52 X. Q. Liu, F. Wang, R. Aizen, O. Yehezkeli and I. Willner, *J. Am. Chem. Soc.*, 2013, **135**, 11832–11839.
53 J. P. Xie, Y. G. Zheng and J. Y. Ying, *J. Am. Chem. Soc.*, 2009, **131**, 888–889.
54 J. R. Lakowicz, *Principles of Fluorescence Spectroscopy*, Springer, 2006.
55 H. X. Chang, L. H. Tang, Y. Wang, J. H. Jiang and J. H. Li, *Anal. Chem.*, 2010, **82**, 2341–2346.
56 H. J. Forman, H. Q. Zhang and A. Rinna, *Mol. Aspects Med.*, 2009, **30**, 1–12.
57 Y. L. Xianyu, Y. Z. Y. Xie, N. X. Wang, Z. Wang and X. Y. Jiang, *Small*, 2015, **11**, 5510–5514.
58 R. Franco and J. A. Cidlowski, *Cell Death Differ.*, 2009, **16**, 1303–1314.
59 L. A. Herzenberg, S. C. DeRosa, J. G. Dubs, M. Roederer, M. T. Anderson, S. W. Ela, S. C. Deresinski and L. A. Herzenberg, *Proc. Natl. Acad. Sci. U. S. A.*, 1997, **94**, 1967–1972.
60 D. M. Townsend, K. D. Tew and H. Tapiero, *Biomed. Pharmacother.*, 2003, **57**, 145–155.
61 X. F. Jia, J. Li and E. K. Wang, *Chem.–Eur. J.*, 2012, **18**, 13494–13500.
62 N. Li, W. Diao, Y. Y. Han, W. Pan, T. T. Zhang and B. Tang, *Chem.–Eur. J.*, 2014, **20**, 16488–16491.
63 S. Banerjee, S. Kar, J. M. Perez and S. Santra, *J. Phys. Chem. C*, 2009, **113**, 9659–9663.
64 R. Banerjee, *J. Biol. Chem.*, 2012, **287**, 4397–4402.
65 M. G. Tian, F. Q. Guo, Y. M. Sun, W. J. Zhang, F. Miao, Y. Liu, G. F. Song, C. L. Ho, X. Q. Yu, J. Z. Sun and W. Y. Wong, *Org. Biomol. Chem.*, 2014, **12**, 6128–6133.
66 (*a*) L. Ding, J. You, R. Kong and F. Qu, *Anal. Chim. Acta*, 2013, **793**, 19–25; (*b*) H. Pei, S. Zhu, M. Yang, R. Kong, Y. Zheng and F. Qu, *Biosens. Bioelectron.*, 2015, **74**, 909–914; (*c*) Y. Ding, L. Shi and H. Wei, *Chem. Sci.*, 2015, **6**, 6361–6366; (*d*) H. Cheng, X. Qiu, X. Zhao, W. Meng, D. Huo and H. Wei, *Anal. Chem.*, 2016, **88**, 2937–2943.

